Cretaceous Research 34 (2012) 10–25

Contents lists available at SciVerse ScienceDirect

Cretaceous Research

journal homepage: www.elsevier.com/locate/CretRes

Fault-controlled stratigraphy of the Late Cretaceous Abiod Formation at Ain Medheker (Northeast Tunisia)

Saloua Bey[a,b], Jochen Kuss[a,*], Isabella Premoli Silva[c], M. Hedi Negra[b], Silvia Gardin[d]

[a] Universität Bremen – FB 5, P.O. Box 330440, D-28355 Bremen, Germany
[b] Universite Tunis El Manar II, Faculté des Sciences de Tunis, UR Pétrologie sédimentaire et cristalline, Tunisia
[c] Universita di Milano, Dipartimento di Scienze della Terra, Milan, Italy
[d] University of Paris VI, CNRS UMR 7207 "Centre de recherche sur la paleobiodiversie et les paleoenvironments – CR2P", case 104, Paris, France

ARTICLE INFO

Article history:
Received 29 December 2010
Accepted in revised form
12 September 2011
Available online 22 September 2011

Keywords:
Biostratigraphy
Isotope stratigraphy
Campanian
Maastrichtian
Tunisia
Tectonics
Mass-flow

ABSTRACT

The palaeogeographic setting of the studied Ain Medheker section represents an Early Campanian to Early Maastrichtian moderately deep carbonate shelf to distal ramp position with high rates of hemipelagic carbonate production, periodically triggered by mass-flow processes. Syndepositional extensional tectonic processes are confirmed to the Early Campanian. Planktonic foraminifera identified in thin sections and calcareous nannofossils allow the identification of the following biozones: *Globotruncanita elevata*, *Contusotruncana plummerae* (replacing former *Globotruncana ventricosa* Zone), *Radotruncana calcarata*, *Globotruncana falsostuarti*, and *Gansserina gansseri*. The following stable C-isotope events were identified: the Santonian/Campanian boundary Event, the Mid-Campanian Event, and the Late Campanian Event. Together with further four minor isotopic events, they allow for correlation between the western and eastern realms of Tunisia. Frequently occurring turbidites were studied in detail and discussed in comparison with contourites.

1. Introduction

Northeast and east Central Tunisia was located on the southwestern shelf of the Tethyan Ocean during the Cretaceous Period. It forms the western part of the Pelagian Shelf, a geological province that includes mainly the Tunisian offshore areas (as far as Malta and northwestern Libya; Klett, 2001). During the Late Cretaceous to Neogene interval, periods of extensional tectonics were followed by structural inversion, reverse or thrust faulting, whereby Triassic evaporites provided a "décollement surface" (Guiraud, 1998). In Late Cretaceous times, a shallow submarine swell ran nearly parallel to a major tectonic element, the "North–South Axis", separating the Tunisian Trough (west of the swell) from the Pelagian Shelf to the east (Fig. 1A).

The "North–South Axis"-tectonic element represents a 100-km-long deformation front of the Atlas Mountains in central Tunisia and consists of NE–SW to NNE–SSW-trending tight folds and thrusts, reactivated during the African–European collision in Middle Miocene time (Anderson, 1996). Adjacent to the Pelagian Platform, thrust structures are affected later by strike-slip faults (Fig. 1B). The complex structural evolution of the "North–South Axis"-tectonic element was interpreted by Ouali et al. (1987) and Boccaletti et al. (1988) as a transpressive 'flower' structure, generated during sinistral strike-slip on an inferred N–S-trending basement fault. These authors have proposed a Late Miocene to Early Pliocene age for the faulting and folding and therefore interpreted the "North–South Axis"-tectonic element as a post-collisional structure. Bouaziz et al. (2002) interpreted the "North–South Axis"-tectonic element as resulting from the polyphase reactivation of an inherited Pan-African or Palaeozoic lineament. A major extensional stage with WNW–ESE striking direction was described from the Campanian–Early Maastrichtian, documented by a NW–SE to NNW–SSE conjugate normal fault system that cut the Campanian carbonates and form syndepositional features of the Abiod Formation in the folded Atlasic domain (Bouaziz et al., 2002).

The studied Abiod succession at Ain Medheker is situated at the eastern flank near the northern termination of the "North–South Axis"-tectonic element (Fig. 1B). A major syndepositional normal fault was discovered in the lower part of the outcrop, indicating Early Campanian extensional tectonic movements. They are comparable to similar extensional processes that affected the whole North African margin, originating from NW–SE to NNW–SSE striking basins, as described by Baird et al. (1996). In defined alternating intervals of the whole succession, slumpings and turbidites reflect

* Corresponding author. Tel.: +49 42121865250; fax: +49 42121865279.
E-mail address: kuss@uni-bremen.de (J. Kuss).

0195-6671/$ – see front matter © 2011 Elsevier Ltd. All rights reserved.
doi:10.1016/j.cretres.2011.09.008

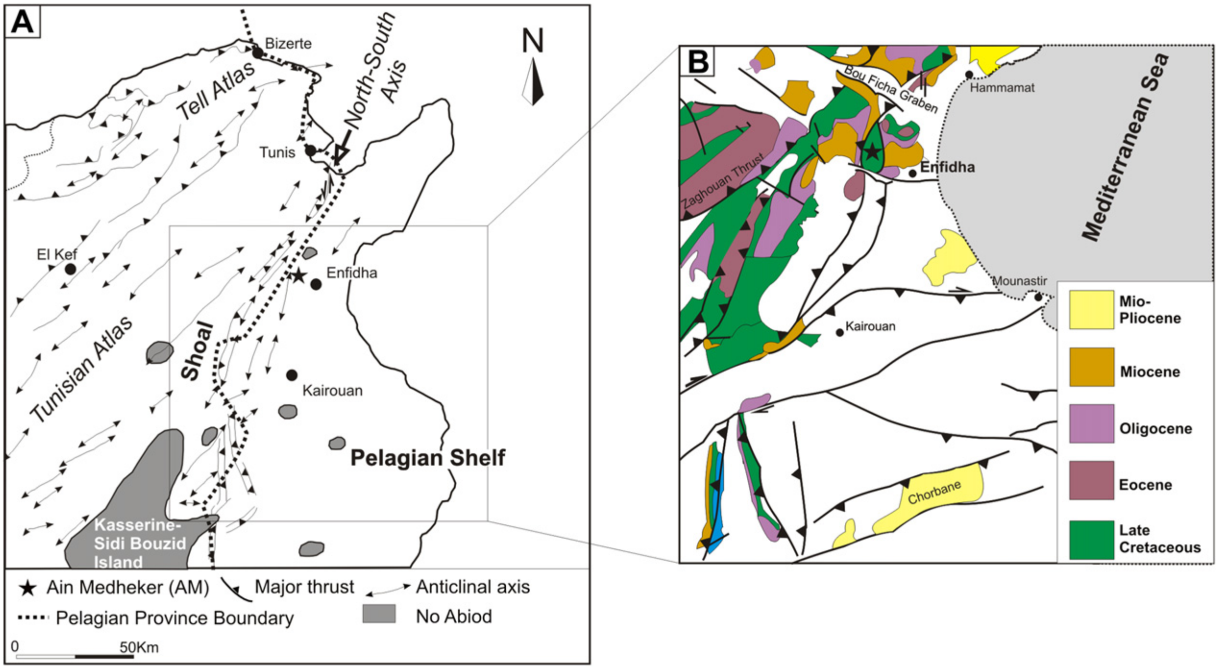

Fig. 1. A, major tectonic units of northeast Tunisia (after Anderson, 1996) and thickness distribution of the Abiod Formation (after Hennebert et al., 2009). Asterisk indicates the position of the studied section at Ain Medheker. B, simplified geological map (after Khomsi et al., 2009) around Enfidha with the studied section of Ain Medheker (asterisk).

imprints of syndepositional reworking of (hemi) pelagic carbonaceous sediments on a palaeo-slope. The analysis of planktonic foraminifera allows for a high-resolution biostratigraphic framework, supported by stable isotope-geochemistry data. The latter have been widely used as in important tool for stratigraphic correlation in Late Cretaceous pelagic and hemipelagic settings (Scholle and Arthur, 1980; Jarvis et al., 2002, 2006; Jacobs et al., 2005) and enable us to refine the stratigraphic concepts of the studied section.

The main goals of this paper are to: (1) describe the characteristics of the stratigraphic record of a Late Cretaceous submarine fault-controlled half-graben and the corresponding downcurrent mass-flow processes; (2) analyze the stratigraphic architecture of the Abiod Formation at Ain Medheker; (3) date the main events recorded in it; (4) to identify the processes controlling turbidite sedimentation; and (5) to integrate all data into a regional and supraregional stratigraphic framework.

These data will provide a deeper understanding of the stratigraphic evolution of the Late Cretaceous Abiod Formation, syndepositional tectonic movements that are related to stages of extensional tectonics, and will contribute to interpretations on the evolution of the Late Cretaceous Pelagian Shelf. The ultimate objective of this study is to integrate outcrop geological data and descriptions from similar areas to develop a tectono-sedimentary model explaining depositional processes during the Campanian–Early Maastrichtian period.

2. Geological setting

The Abiod Formation (Early Campanian–Early Maastrichtian) of Tunisia exhibits varying thicknesses and facies from the south to the north. In the Kasserine area (central Tunisia), the thickness is highly reduced and the Abiod Formation includes conglomeratic gravity flow deposits (Negra, 1994) and local rudist-bearing limestones (Khessibi, 1978; M'Rabet et al., 1986; Negra, 1986, 1995; Negra and Purser, 1989, 1995; Ben Ferjani et al., 1990; Negra et al., 1995; Negra and Gili, 2004), or is even missing in the Kasserine-Sidi Bouzid Island (Negra et al., 1995; Fig. 1A). Further to the south (Gafsa area), the Abiod Formation consists of bioclastic limestones, intercalated with sandy, dolomitic and evaporitic intervals (Abdallah, 1987; Negra and M'Rabet, 1994; Chaabani, 1994), indicating the proximity to the southern Saharan Platform. In the southernmost areas (Chotts), the Abiod facies becomes more proximal with lagoonal to intertidal–subtidal environments.

Based on thickness variations of the Abiod Formation, Hennebert et al. (2009) proposed two elongated shoals in central East Tunisia (Fig. 1A): the first runs along the northern prolongation of the Kasserine Island, nearly parallel to the "North–South Axis"-tectonic element, with a subsiding basin (Tunisian Trough) to the west, where the Abiod Formation exceeds 600 m of pelagic and hemipelagic chalks and marls (Burollet and Ellouz, 1984; Ben Ferjani et al., 1990); the second is situated to the east of Kasserine Island, extending over the Pelagian Shelf. Both shoals exhibit several highs that are indicated by circular areas without Abiod Formation (Fig. 1A).

The studied section AM (Ain Medheker) is located to the west of an active quarry at the village of Ain Medheker (ca.10 km west of Enfidha). It is near the eastern boundary of the "North–South Axis"-tectonic element, therefore representing also the eastern flank of the first shoal (Fig. 1A,B).

3. Material and methods

The studied section AM comprises a 115-m-thick succession of limestones and marly or argillaceous limestones. The Abiod Formation (105 m) is sandwiched between the upper Aleg Formation (below) and the El Haria Formation (above; Fig. 2). Our detailed microfacies, biostratigraphy and chemostratigraphy studies were carried out on 130 samples that were collected bed-by-bed; moreover, the textures of both, hemipelagic carbonates and intercalated turbiditic layers of the Abiod Formation (including the transition to the underlying/overlying formations) was documented. A total of 72 thin sections were prepared from limestones to determine the microfossils and the microfacies characteristics. The percentages of the main components were estimated by means of point counting (see Fig. 2). Planktonic foraminifera are the most

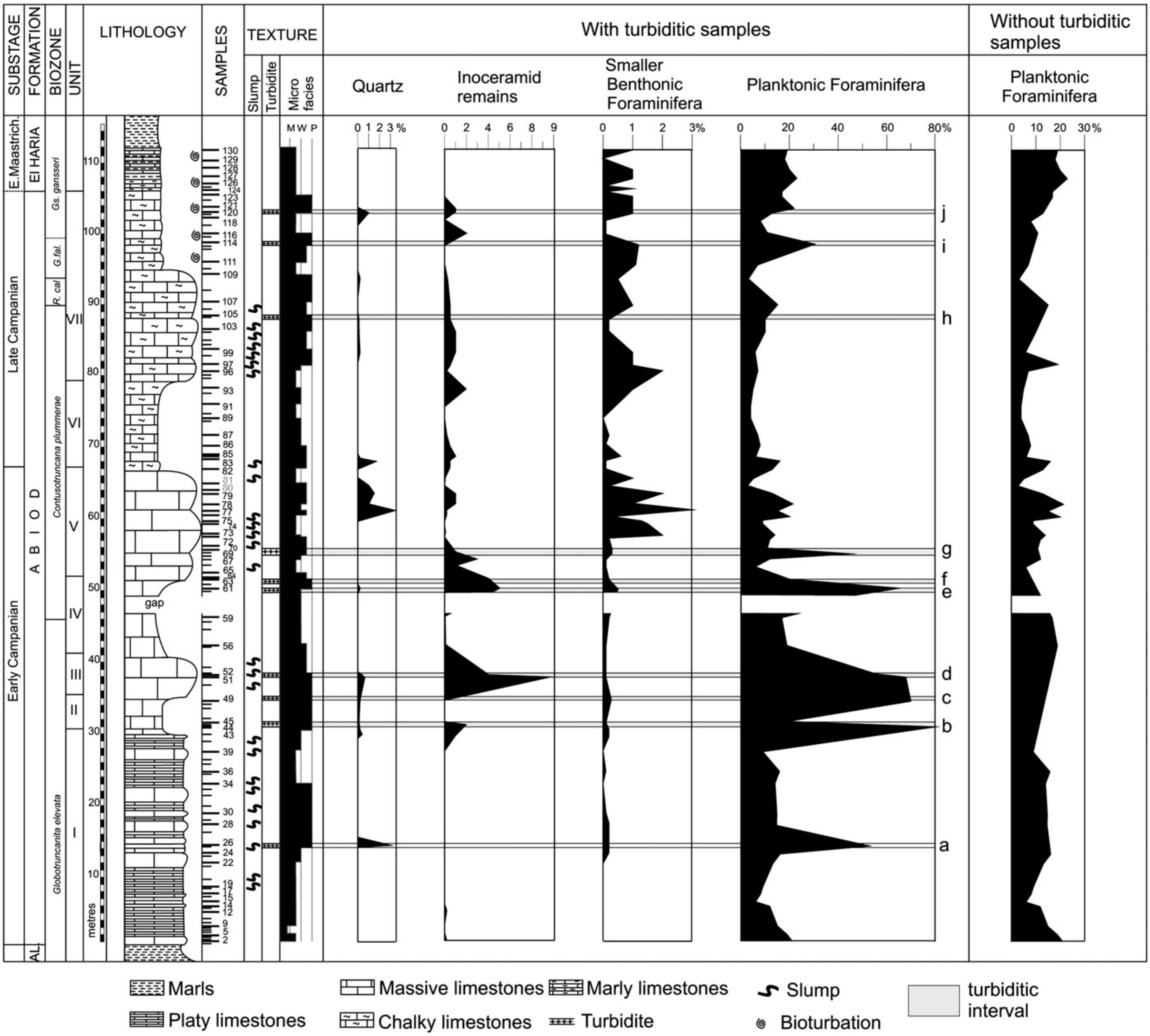

Fig. 2. Sedimentologic characteristics of the 105-m-thick Abiod Formation at Ain Medheker, composed of different carbonate lithologies that are summarized in field units I–VII (compare Figs. 5, 6). A sharp boundary to the underlying Aleg Formation (composed of dark marls), contrasts with a gradual transition to the overlying El Haria Formation (composed of dark limestone-marl alternations). Numbered samples (broad bulks) refer to the thin sections of (hemi)pelagic limestones studied. Four turbidite-rich intervals are highlighted (summarizing one to three single turbidite beds a–j); they alternate with slump-rich intervals. The distribution of the major components is often related to slope events (turbidites-contourites and/or slumps). The right-hand column refers to the semi-quantitative distribution of planktonic foraminifera without turbiditic samples. Microfacies: M, mudstone; W, wackestone; P, packstone (the varying content of mainly micritic matrix is not considered).

Table 1
Distribution and quantification (specimens/210 fields of view) of key and marker nannofossil species in the samples studied.

	A. parcus expansus	*A. parcus parcus*	*A parcus constrictus*	*A. cymbiformis*	*E. eximius*	*R. anthophorus*	*O. campanensis*	*A. regularis*	*C. verbeckii*
AM 23		3	3	2	16	2		2	1
AM 14		4	6		13	3		1	3
AM 13		5	9		15	4	1	2	2
AM 10		4	4		11	1		1	1
AM 7		2	4		12	3	1	1	
AM 5		2	3		10	2		1	
AM 1	1	5	2	1	11	2			

Table 2
Database of planktonic foraminifera of section AM.

SAMPLES N°	AM2	AM5	AM9	AM14	AM15	AM17	AM19	AM22	AM24	AM28	AM30	AM34	AM36	AM39	AM43	AM44	AM45	AM49	AM51	AM52	AM56	AM59	AM61	AM63	AM64	AM65	AM67	AM69	AM70	AM72	AM73	AM74	AM75	AM77	AM78	AM79	AM80	AM81	AM82	AM83	AM85	AM86	AM87	AM89	AM91	AM93	AM96	AM97	AM99	AM103	AM105	AM107	AM109	AM111	AM114	AM116	AM118	AM120	AM121	AM123	AM124	AM126	AM127	AM128	AM129	AM130
Globotruncana arca	•	•	•						•		•	•	•								•	•	•	•							•					•	•		•	•	•	•	•	•	•	•	•						•			•	•	•				•				
Pseudotextularia nuttalli	•		•							•																					•						•		•		•		•	•	•	•	•	•									•	•								
Globotruncanita elevata		•		•		•			•		•		•	•						•				•																•								•																		
Contusotruncana fornicata	•	•	•									•									•										•				•		•		•	•			•	•	•	•	•							•				•								•
Globotruncanita stuartiformis		•				•		•	•	•	•	•	•	•			•					•		•							•	•	•			•			•		•	•	•		•	•	•	•				•	•			•	•	•	•			•	•	•	•	•
Globigerinelloides messinae		•							•																												•						•																						•	
Globotruncana linnieana		•	•		•			•	•	•	•	•	•				•		•				•	•							•									•		•	•		•	•		•				•	•			•	•	•								
Globotruncana hilli		•	•					•	•		•		•				•		•		•	•	•								•		•			•			•			•					•						•				•			•						•
Globotruncana lapparenti			•					•	•	•											•										•					•				•					•	•										•	•									
Globotruncana bulloides			•					•	•		•		•										•							•	•	•				•			•	•	•	•		•	•	•	•						•			•	•			•						
Archaeoglobigerina cretacea			•								•																				•								•	•																•				•	•				•	
Dicarinella sp.			•																																																															
Marginotruncana sp.				•		•			•	•																																																								
Schackoina cenomana					•	•	•																																																											
Ventilabrella glabrata					•																																																													
Globigerinelloides ultramicrus						•	•		•			•		•			•			•	•		•		•						•			•	•								•							•	•	•	•								•				•	
Globigerinelloides multispinus							•																		•																														•											
Ventilabrella sp.							•			•	•		•		•		•	•		•	•		•	•		•		•	•	•	•				•	•		•	•	•	•																									
Heterohelix globulosa								•		•	•	•																			•	•																																		
Marginotruncana pseudolinneiana								•	•																																																									
Marginotruncana sigali									•																																																									
Globigerinelloides prairiehillensis									•	•														•									•						•	•	•					•					•										•					•
Heterohelix striata										•			•																		•																																			
Heterohelix punctulata															•				•			•						•								•											•		•			•														
Heterohelix reussi														•		•																																																		
Archeoglobigerina blowi																	•																						•	•																										
Contusotruncana patelliformis																				•											•								•	•	•		•	•	•	•	•			•		•		•		•	•		•	•		•	•		•	•
Pseudoguembelina costulata																					•	•	•			•				•		•	•				•															•					•		•		•		•	•		•
Contusotruncana plummerae																						•					•			•	•		•	•	•		•		•	•	•	•	•				•		•											•						
Rugoglobigerina rugosa																							•																•										•		•								•	•			•			•
Globotruncana orientalis																								•							•	•							•	•			•			•		•					•						•						•	
Globotruncana tricarinata																															•						•																													
Globigerinelloides alvarezi																															•								•				•				•		•		•									•					•	
Globotruncanita atlantica																															•					•	•			•						•	•		•		•															
Globotruncana rosetta																															•																											•								
Ventilabrella eggeri																																	•																																	
Globotruncana mariei																																											•										•				•			•						
Radotruncana subspinosa																																				•			•				•	•	•		•	•		•		•	•													
Globigerinelloides subcarinatus																																																																•		
Globotruncana ventricosa																																							•		•	•	•				•	•			•		•			•	•	•								
Globotruncana insignis																																							•	•	•	•					•	•				•	•							•						
Globigerinelloides bollii																																									•		•	•					•		•		•													
Pseudotextularia elegans																																											•						•		•			•			•	•	•			•				•
Globotruncanella sp.																																																	•												•					
Globotruncanella havanensis																																																	•									•	•		•					
Globotruncana falsostuarti																																																		•	•	•						•								
Radotruncana calcarata																																																				•	•													
Rugoglobigerina hexacamarata																																																						•		•	•		•							•
Rugoglobigerine pennyi																																																						•		•					•		•	•	•	
Planoglobulina carseyi																																																						•		•	•	•	•			•	•		•	•
Globotruncanita petersi																																																						•						•	•					
Rugoglobigerina macrocephala																																																							•											
Ventilabrella multicamerata																																																								•		•		•						
Globotruncanita angulata																																																								•			•	•	•					
Gansserina gansseri																																																								•	•	•				•				
Planoglobulina acervulinoides																																																									•	•	•	•	•	•	•	•	•	•
Globotruncanita stuarti																																																									•	•	•	•		•	•	•	•	•
Globotruncana aegyptiaca																																																										•								
Gansserina wiedenmayeri																																																												•	•	•	•			
Contusotruncana contusa																																																														•				
Rugoglobigerina milamensis																																																														•				•
Planoglobulina sp.																																																																		•

Table 3
Database of measured $\delta^{13}C$ data.

Sample	13/12-C	Sample	13/12-C	Sample	13/12-C	Sample	13/12-C	Sample	13/12-C
AM1	2,26	AM27	1,99	AM53	2,07	AM79	1,94	AM105	1,90
AM2	2,22	AM28	2,25	AM54	1,97	AM80	2,00	AM106	2,07
AM3	2,27	AM29	2,04	AM55	2,02	AM81	2,04	AM107	1,80
AM4	2,12	AM30	2,19	AM56	1,70	AM82	2,03	AM108	1,85
AM5	2,06	AM31	2,12	AM57	1,91	AM83	2,09	AM109	1,73
AM6	2,11	AM32	2,09	AM58	1,99	AM84	2,02	AM110	1,90
AM7	2,14	AM33	2,09	AM59	1,93	AM85	2,03	AM111	1,44
AM8	2,21	AM34	2,24	AM60	1,98	AM86	2,09	AM112	1,86
AM9	2,28	AM35	2,29	AM61	1,66	AM87	2,10	AM113	1,72
AM10	2,25	AM36	2,31	AM62	2,00	AM88	2,06	AM114	1,42
AM11	2,31	AM37	2,28	AM63	2,06	AM89	1,88	AM115	1,58
AM12	2,25	AM38	1,95	AM64	1,97	AM90	2,10	AM116	1,61
AM13	2,34	AM39	2,09	AM65	1,93	AM91	2,16	AM117	1,57
AM14	2,25	AM40	2,03	AM66	1,88	AM92	1,96	AM118	1,52
AM15	2,17	AM41	1,94	AM67	2,07	AM93	1,95	AM119	1,44
AM16	2,24	AM42	2,01	AM68	2,03	AM94	2,05	AM120	1,48
AM17	2,07	AM43	2,03	AM69	1,73	AM95	2,11	AM121	1,65
AM18	2,16	AM44	1,95	AM70	2,00	AM96	1,93	AM123	1,70
AM19	1,85	AM45	1,67	AM71	2,08	AM97	2,13	AM124	1,68
AM20	2,14	AM46	1,93	AM72	2,12	AM98	2,20	AM125	1,75
AM21	1,99	AM47	2,08	AM73	1,86	AM99	2,08	AM126	1,66
AM22	1,86	AM48	2,07	AM74	1,99	AM100	2,06	AM127	1,47
AM23	2,02	AM49	1,94	AM75	1,98	AM101	2,09	AM128	1,67
AM24	1,88	AM50	2,02	AM76	1,86	AM102	2,14	AM129	1,68
AM25	1,96	AM51	2,05	AM77	1,94	AM103	2,09	AM130	1,32
AM26	2,06	AM52	1,98	AM78	1,69	AM104	2,14		

frequent constituents and were classified taxonomically, based on the criteria defined by Premoli Silva and Sliter (1995) and Premoli Silva and Verga (2004).

In order to strengthen the age assignment of the base of Ain Medheker section, seven samples from the basal limestones were examined for their nannofossil content. The study of calcareous nannofossils was conducted by means on standard processed smear slides and specimens were identified under light microscope at 1250× magnification. Biostratigraphically important species were quantified along two traverses of each smear slide which correspond to approximately 210 fields of view (see Table 1).

A total of 130 bulk rock samples (with an average spacing of ca. 0.8 m) were analyzed for stable carbon isotopes (Table 3). To avoid diagenetic alteration, all geochemical samples were selected from the micritic parts of the limestones. The stable isotope composition was measured using a Finnigan mass spectrometer at MARUM Bremen. The results are expressed in the common δ-notation in per mille relative to PDB (PeeDee belemnite) standard and are compared with stable carbon isotope data described by Jarvis et al. (2002) from age-equivalent strata of El Kef (western Central Tunisia) and of Trunch (UK).

4. Results

4.1. Lithology and regional stratigraphy

The white limestones of the Abiod Formation in Ain Medheker are underlain by dark grey limestones and marls of the Aleg Formation (Late Turonian–Late Santonian) and overlain by rhythmic alternations of dark marls and limestones comprising the lower part of the clayey El Haria Formation (Early Maastrichtian–Paleocene) (Fig. 2). The base of the Abiod Formation is represented by white–grey limestones (unit I), while the top is defined by a gradual transition to dark limestones and marls of the El Haria Formation. Mabrouk et al. (2006) discussed an unconformity between the Aleg and Abiod Formations, based on subsurface studies offshore Tunisia.

Several authors described a tripartite Abiod Formation consisting of two calcareous units separated by a marly member (M'Rabet et al., 1986; Negra and Purser, 1989; Negra et al., 1995), which was recently refined by Robaszynski and Mzoughi (2010). In section Ain Medheker, however, this tripartite subdivision cannot be applied, but the Abiod Formation was subdivided into seven lithostratigraphic units (I–VII) (Fig. 2). Unit I is split into platy and marly limestones at the base and massive limestones above, with slumping structures mainly in the upper part (Fig. 2). Unit II consists of thick-bedded limestones, with intercalations of massive, slumped, limestone packages in the upper part (unit III; Fig. 6C); thin turbiditic layers occur in both units. Similarly, units IV and V are composed of thick-bedded (IV) and massive slumped packages (V) with turbidites (Fig. 6E). Unit VI comprises well-bedded chalky limestones, while unit VII above is split into massive chalky limestones with major slumps at the base that are overlain by bedded chalky and marly limestones with conspicuous ichnofossils (*Helminthoida* sp.). The upper boundary to the rhythmically alternating dark marls and limestones of the El Haria Formation is gradational.

Chronostratigraphically, the Abiod Formation spans an Early Campanian–Early Maastrichtian interval in the eastern parts of Central Tunisia, near El Kef and Elles (Li and Keller, 1998; Li et al., 1999, 2000; Jarvis et al., 2002; Robaszynski and Mzoughi, 2004, 2010; Hennebert et al., 2009). In the studied section AM, an Early Campanian age (*Globotruncanita elevata* Zone) was attributed to the basal beds of the Abiod Formation, while the top beds lie within the *Gansserina gansseri* Zone of earliest Maastrichtian age (see below, Fig. 3).

4.2. Biostratigraphy: planktonic foraminifera

The study of planktonic foraminifera from the Ain Medheker section was conducted using two-dimensional well-cut views from thin sections. Specimens were identified taking into account the test size, profile shape and type of margin, growth-ratio patterns, chamber size, size of umbilicus, wall thickness, and ornamentation. However, it is worth mentioning that in thin sections rare species may not be detected and ranges of taxa may appear shorter than those that can be obtained from washed residues, a method that concentrates the specimens.

The 72 thin sections examined yielded highly diverse, mostly abundant and well preserved planktonic assemblages (Figs. 7, 8).

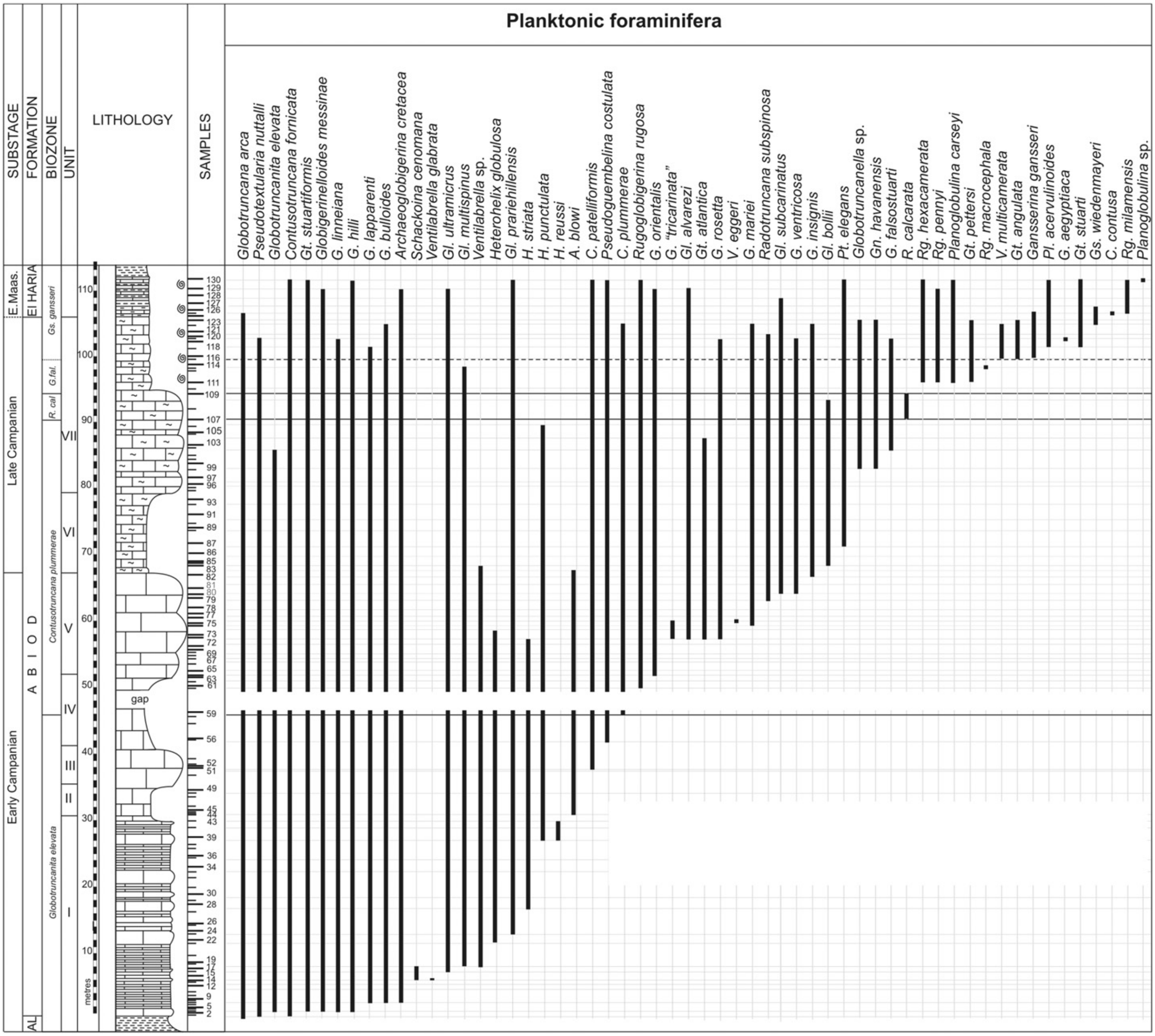

Fig. 3. Distribution of planktonic foraminifera identified in the thin sections studied. Biozonal scheme after Robaszynski et al. (1984), supplemented by the *Contusotruncana plummerae* Zone (replacing the former *Globotruncana ventricosa* Zone). Note that Premoli Silva and Sliter (1995, 1999) used the *Globotruncanella havanensis* Zone and *Globotruncana aegyptiaca* Zone instead of *Globotruncana falsostuarti* Zone. *A, Archaeoglobigerina*; *C, Contusotruncana*; *G, Globotruncana*; *Gl, Globigerinelloides*; *Gn, Globotruncanella*; *Gs, Gansserina*; *G, Globotruncanita*; *H, Heterohelix*; *Pl, Planoglobulina*; *Pt, Pseudotextularia; R, Radotruncana*; *Rg, Rugoglobigerina*; *V, Ventilabrella*. For legend see Fig. 2.

Fifty-seven species belonging to 15 genera could be identified by comparison with the extensive thin-section illustrations provided by Premoli Silva and Sliter (1995), Robaszynski et al. (2000), and Premoli Silva and Verga (2004) among others.

Planktonic foraminiferal assemblages throughout the section are dominated by the keeled genera *Globotruncanita, Globotruncana, Radotruncana, Contusotruncana* associated with less common genera *Globotruncanella, Gansserina, Archaeoglobigerina, Globigerinelloides, Rugoglobigerina,* some heterohelicids (*Heterohelix*, most common), *Pseudotextularia, Pseudoguembelina, Ventilabrella, Planoglobulina*, and rare *Schackoina* (see Fig. 3). For genus abbreviations see caption to Fig. 3.

On the basis of the stratigraphic distribution of the species identified (see Fig. 3), five biozones combining the standard schemes (i.e., Caron, 1985; Sliter, 1989; Premoli Silva and Sliter, 1995; Robaszynski et al., 2000; Petrizzo et al., 2011) could be recognized at Ain Medheker with minor modifications. They are (in stratigraphic order), the *Globotruncanita elevata, Globotruncana ventricosa, Radotruncana calcarata, Globotruncana falsostuarti*, and *G. gansseri* zones spanning the Early Campanian to the Early Maastrichtian. The modifications to the standard zonation concern the identification of the *G. elevata*/*G. ventricosa* zonal boundary, which is defined by the lowest occurrence (LO) of *G. ventricosa*. Firstly, the stratigraphic range of this taxon has been proved to be diachronous at different latitudes and the appearance of *G. ventricosa* at Tethyan latitudes is markedly delayed with respect to the southern oceans (Petrizzo, 2000, 2001, 2003). Secondly, the taxonomic concept of *G. ventricosa* has changed through the years after the revision of the globotruncanids by Robaszynski et al. (1984), who included in

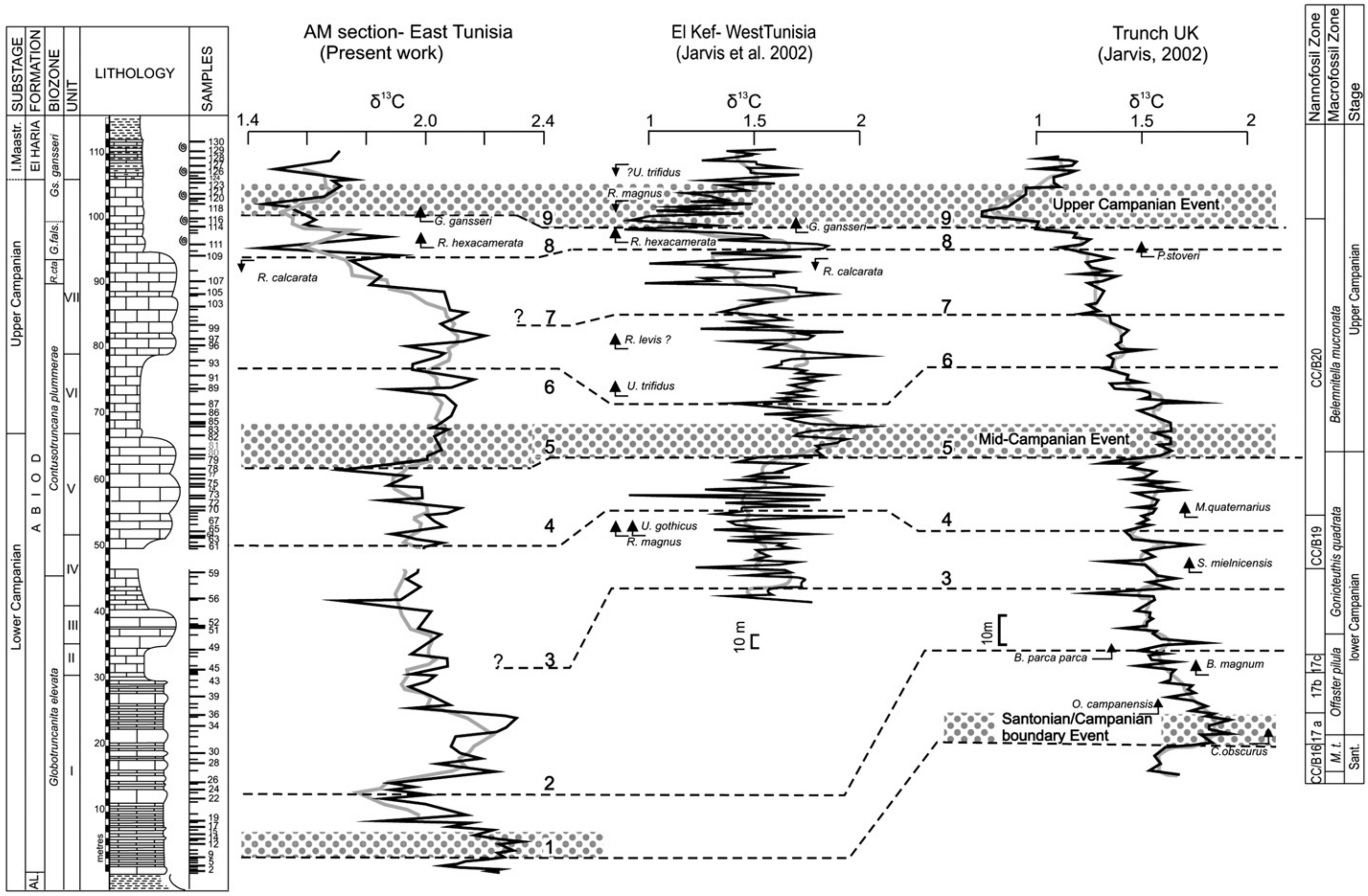

Fig. 4. Distribution of δ^{13}C-values (whole-rock samples) from Ain Medheker (AM) in comparison with those from West Tunisia (El Kef) and southern England (Trunch). Nine lines of correlation (stippled lines) are based on Jarvis et al. (2002) and allow specification of the biostratigraphic age model of Fig. 3. For Legend see Fig. 2.

G. ventricosa also forms transitional between *Globotruncanita linneiana* and the true, plano-umbilically convex *G. ventricosa* (i.e., *Globotruncanita tricarinata* auctorum). Consequently, the LO of *G. ventricosa* resulted in being much lower than the appearance of its typical forms, at least at low latitudes. It is worth noting that the identification of zonal boundaries based on transitional forms is not an easy task and can be very subjective; in addition, if identifications are conducted on thin sections, the placement of any zonal boundary can end up being apparently diachronous.

At Kalaat Senan, Robaszynski et al. (2000) identified a “subzone of abundant *G. ventricosa*” in the upper part of their *G. ventricosa* Zone, a fact suggesting that the real appearance of this taxon, when it is much less common, is difficult to detect especially in thin section. Recently, Petrizzo et al. (2011), in their comparative biostratigraphic study on planktonic foraminiferal distribution from some widespread localities, highlighted (1) the absence of *G. ventricosa* at the stratigraphic level at which is supposed to occur first in the Tethyan area and (2) the presence of transitional forms resembling *G. ventricosa* and erroneously used to identify the base of the *G. ventricosa* Zone, meanwhile suggesting the appearances of *Globotruncanita atlantica*, *Contusotruncana plummerae* and the highest occurrence (HO) of *Hendersonites carinatus* (formerly *Heterohelix carinata*) as potentially good bioevents for regional and global correlation. Owing to the difficulty of using *G. ventricosa* as zonal marker in tropical and subtropical areas, these authors proposed a new zone based on the first appearance of *C. plummerae*, replacing the long *G. ventricosa* Zone of the standard zonation.

At section AM the appearance of *C. plummerae* is recorded in sample AM59, followed by that of *Gt. atlantica* in sample AM73, whereas *H. carinatus* was not found. In addition, the LO of *C. plummerae* is preceded, ca. 10 m below, by the LO of *Contusotruncana patelliformis* in sample AM52 within unit III (see Fig. 3, Table 2), the LO of which, however, appears delayed in section AM in comparison with other, even Tunisian, sections (see Robaszynski et al., 2000; Robaszynski and Mzoughi, 2010; Petrizzo et al., 2011).

Taking this finding into account, and in agreement with Petrizzo et al. (2011), the *Gt. elevata*/*G. ventricosa* zonal boundary is here tentatively drawn at the level of the LO of *C. plummerae* (sample AM59). Accordingly, the former *G. ventricosa* Zone is replaced here by the *C. plummerae* as defined by Petrizzo et al. (2011).

Globotruncanita elevata Interval Zone

New definition: the interval from the highest occurrence (HO) of *Dicarinella asymetrica* to the LO of *Globotruncana plummerae*.

The base of the Abiod Formation in section AM can be attributed to the *G. elevata* Zone due to the presence of the nominal taxon along with *Globotruncanita stuartiformis* (Fig. 8A–D) and the absence of dicarinellids and marginotruncanids (see Fig. 3). The assemblages are dominated by double-keeled specimens of *Globotruncana* and single-keeled *Globotruncanita*. Other species identified are *Contusotruncana fornicata, Pseudotextularia nuttalli* (Fig. 8L,M), *Archaeoglobigerina cretacea* (Fig. 8N), followed by *Heterohelix globulosa* (Fig. 8R,S), *Globigerinelloides prairiehillensis*, and *Heterohelix striata*. *C. patelliformis* (Fig. 8Q) appears in the upper

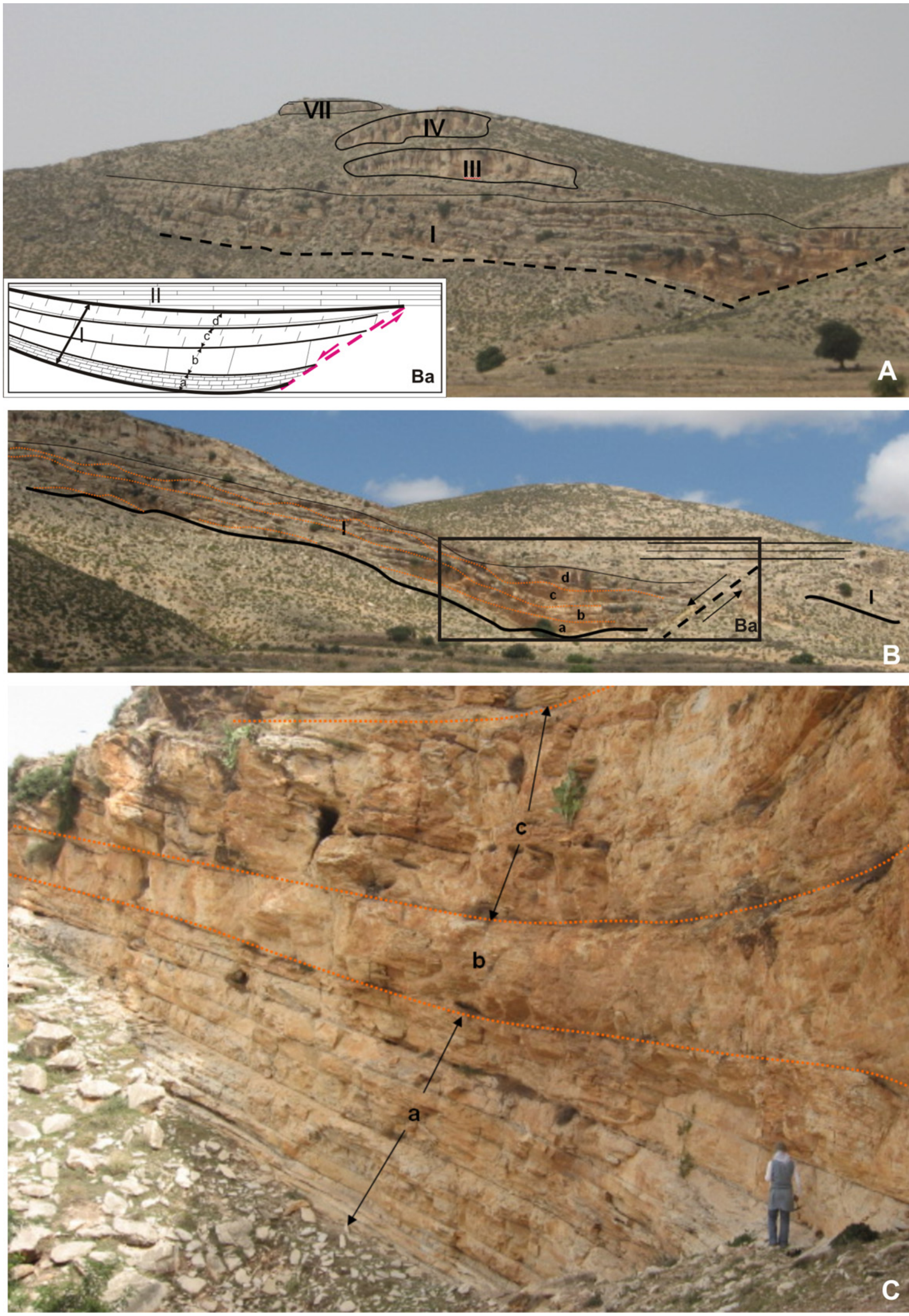

Fig. 5. Field characteristics of the Abiod Formation of Ain Medheker. A, panoramic view of the late Cretaceous strata at Ain Medheker with lithostratigraphic units I–VII representing the Abiod Formation (compare Fig. 2). The lower boundary against the Aleg Formation is covered by younger gravel, except near the fault-related graben structure at the eastern side and at the western part of the outcrop (the sketch in Fig. Ba reflects the half-graben, indicated in B). B, details of unit I with thickening of beds a–d towards the fault, to illustrate the syndepositional tectonic relationships along the normal fault. The conformable succession above (nearly horizontal bedding) starts with unit II. C, carbonates of unit I show an increase in thickness of all three subunits a–c towards the normal fault. Irregular bedding within the subunits reflects slumping and synsedimentary mass movement (see Fig. 6D).

Fig. 6. Field characteristics of the Abiod Formation of Ain Medheker. A, the middle part of the section with major slumpings in units III and V. B, limestones of unit III showing weathered slumping structures with irregular bedding plane and cross-bedding relationships. C, synsedimentary folding (NE–SW striking slump axis) and reworked clasts in the limestones of unit III, indicating a SE-dipping palaeo-slope. D, slumping and cross-bedding relationships within subunits a–b of unit I. E, irregular bedded turbiditic limestones composed of cm-thick packstones (dark grey colour) of unit V. The arrow indicates a bioturbated area within one "turbidite" layer.

part of the zone, while rare *Schackoina cenomana* (Fig. 8G,H) is recorded in the lowermost part.

The upper boundary of the zone is drawn at the level of the LO of *C. plummerae* (Fig. 7E), recorded in sample AM59 within unit IV (see above).

Based on the above definition, the *Gt. elevata* Zone is recorded in ca.45-m-thick limestones of the lower-mid Abiod Formation. An early to early middle Campanian age has been assigned to the *Gt. elevata* Zone by Hardenbol and Robaszynski (1998) and Gradstein et al. (2004).

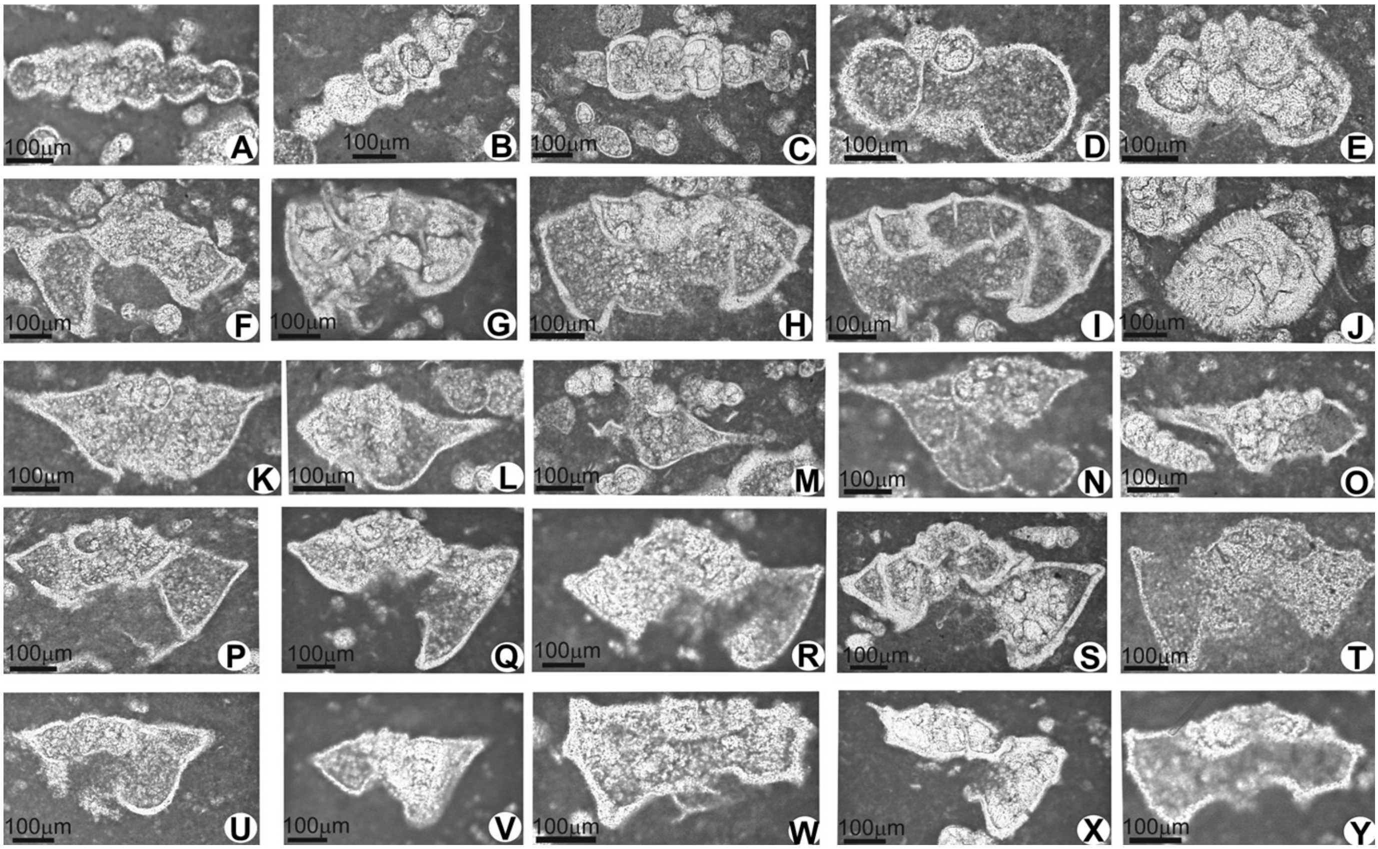

Fig. 7. Stratigraphically important planktonic foraminifera. A, *Planoglobulina acervulinoides* (sample AM111). B, *Planoglobulina acervulinoides* (AM111). C, *Planoglobulina acervulinoides* and *Globotruncanella havanensis* (AM121). D, *Rugoglobigerina pennyi* (AM121). E, *Contusotruncana plummerae* (AM83). F, *Globotruncanita elevata* (AM103). G, *Gansserina gansseri* (AM118). H, *Globotruncana insignis* (AM83). I, *Globotruncana insignis* (AM82). J, *Pseudotextularia elegans* (AM63). K, *Radotruncana calcarata* (AM107). L, *Radotruncana calcarata* (AM107). M, *Radotruncana calcarata* (AM107). N, *Radotruncana calcarata* (AM107). O, *Radotruncana* calcarata (AM107). P, *Globotruncanita stuartiformis* (AM103). Q, *Globotruncanita elevata* (AM97). R, *Globotruncanita elevata* (AM24). S, *Globotruncanita elevata* (AM24). T, *Globotruncanita elevata* (AM19). U, *Radotruncana subspinosa* (AM109). V, *Radotruncana subspinosa* (AM109). W, *Globotruncana ventricosa* (AM109). X, *Globotruncana ventricosa* (AM87). Y, *Globotruncana ventricosa* (AM86).

Contusotruncana plummerae Partial Range Zone

Definition: the interval from the LO of *G. plummerae* (Fig. 7E) to the LO of *R. calcarata* (Fig. 7K–O).

With respect to the LO of *C. plummerae*, which defines the base of the nominal zone, in section AM the lowest true *G. ventricosa* is recorded in the mid part of the *C. plummerae* Zone in the upper part of unit V (sample AM82; see Fig. 3, Table 2), at a level that might be coeval with the base of the "subzone of abundant *G. ventricosa*" identified by Robaszynski et al. (2000) at Kalaat Senan.

The planktonic assemblages in this zone in section AM are characterized overall by the abundance of both genera *Globotruncana* [*G. linnieana, G. arca, G. bulloides* (Fig. 8F), *G. hilli, G. lapparenti, G. mariei, G. orientalis*] and *Globotruncanita* (*Gt. elevata, Gt. stuartiformis*); *H. globulosa, Rugoglobigerina rugosa* (Fig. 8V), and *Pseudogumbelina costulata* (Fig. 8P) are also frequent. Besides *C. plummerae*, *Gt. atlantica* followed by *Radotruncana subspinosa* (Fig. 7U,V) are recorded in the lower part prior to the local LO of true *G. ventricosa* (Fig. 7X, Y). *G. falsostuarti* and *Globotruncanella havanensis* appear in the uppermost part of the zone, whereas *G. elevata* (Fig. 7Q–T) and *G. atlantica* disappear almost at the same levels just prior to the top of the zone. Robaszynski and Mzoughi (2004) considered the HO of *Gt. elevata* as a global bioevent, an assessment not confirmed in their later publication (Robaszynski and Mzoughi, 2010).

In section AM about 45.5-m-thick limestones and marls of the Abiod Formation are attributed to the *G. plummerae* Zone, which can be dated to the middle Campanian according to Hardenbol and Robaszynski (1998) and Gradstein et al. (2004).

Radotruncana calcarata Total Range Zone

Definition: total range zone of the nominal taxon.

The zonal marker *R. calcarata* (Fig. 7K–O) is relatively abundant. The planktonic foraminiferal assemblages of the *R. calcarata* Zone in the studied section are similar to those of the previous *G. plummerae* Zone. Most frequent are various species of the genus *Globigerinelloides* (*Gl. ultramicrus, Gl. bolli*, and *Gl. alvarezi*) together with *R. rugosa* and *Heterohelix punctulata*. In addition to the index species *C. plummerae*, *C. patelliformis, C. fornicata*, and *R. subspinosa* are also well represented in the assemblages.

In section AM only 4 m of marly limestones are assigned to the *R. calcarata* Zone, which was dated to the early Late Campanian by Hardenbol and Robaszynski (1998) and Gradstein et al. (2004).

Globotruncana falsostuarti Partial Range Zone

Definition: the interval from the HO of *R. calcarata* and the LO of *G. gansseri*.

Although this interval had changed its name several times in over fifty years, its definition has remained constant. It was first named as *G. falsostuarti* Zone by Postuma (1971), followed by Robazysinski et al. (1984, 2000). Caron in 1978 changed its name to the *G. havanensis* Zone. Subsequently, Caron in 1985 subdivided the latter biozone (= *G. falsostuarti* Zone of Postuma, 1971) into a lower *G. havanensis* Zone and an upper *Globotruncana aegyptiaca* Zone, a subdivision that was followed by a number of authors (Sliter, 1989; Premoli Silva and Sliter, 1995, 1999; Robaszynski and Caron, 1995; Hardenbol and Robaszynski, 1998). The dual subdivision of

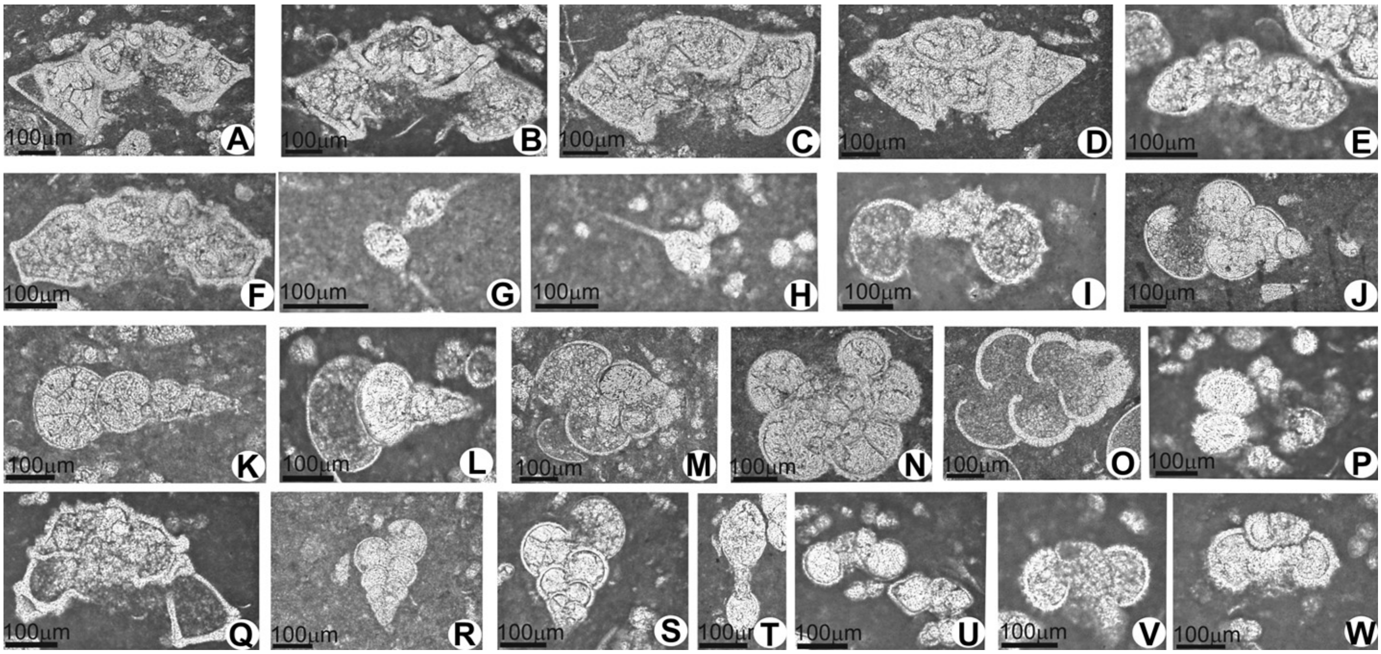

Fig. 8. Stratigraphically important planktonic foraminifera continued. A, *Globotruncanita stuartiformis* (sample AM69). B, *Globotruncanita stuartiformis* (AM59). C, *Globotruncanita stuartiformis* (AM24). D, *Globotruncanita stuartiformis* (AM45). E, *Globotruncanella havanensis* (AM124). F, *Globotruncana bulloides* (AM9). G, *Schackoina cenomana* (AM19). H, *Schackoina cenomana* (AM17). I, *Rugoglobigerina hexacamerata* (AM111). J, *Heterohelix globulosa* (AM85). K, *Heterohelix globulosa* (AM76). L, *Pseudotextularia nuttalli* (AM63). M, *Pseudotextularia nuttalli* (AM76). N, *Archaeoglobigerina cretacea* (AM39). O, *Planoglobulina carseyae* (AM127). P, *Pseudoguembelina costulata* (AM128). Q, *Contusotruncana patelliformis* (AM93). R, *Heterohelix globulosa* (AM39). S, *Heterohelix globulosa* (AM120). T, *Globigerinelloides subcarinatus* (AM124). U, *Archaeoglobigerina blowi* (AM61). V, *Rugoglobigerina rugosa* (AM128). W, *Rugoglobigerina pennyi* (AM128).

this interval could not be applied to the AM assemblages because of the scarcity and scantiness of the index species *G. aegyptiaca*.

In the *G. falsostuarti* Zone of the AM section *Globotruncana, Globotruncanita* and *Contusotruncana* are still the dominating genera. In addition, new taxa such as *Globotruncanita pettersi, Planogobulina carseyae* (Fig. 8O), *Rugoglobigerina hexacamerata* (Fig. 8I), *Rugoglobigerina pennyi* (Fig. 8W) appear within the zone and *Rugoglobigerina macrocephala* at the very top.

The thickness of the *G. falsostuarti* Zone is only 5.5 m in the AM section. According to Hardenbol and Robaszynski (1998) and Gradstein et al. (2004) it can be dated to the middle Late Campanian.

Gansserina gansseri Partial Range Zone

Definition: the interval from the LO of the nominal taxon to the LO of *Abathomphalus mayaroensis*.

The base of the zone in section AM was identified by the appearance of the marker species *G. gansseri* (Fig. 7G) along with the LO of *Ventilabrella multicamerata* and *Globotruncanita angulata*. Other taxa are recorded within this interval, such as *Planoglobulina acervulinoides* (Fig. 7A–C), *Gansserina wiedenmayeri* and *Rugoglobigerina milamensis*; however, all of them display limited ranges. In addition, several species of globotruncanids [*G. linnieana, G. Bulloides* (Fig. 8F), *G. lapparenti, G. mariei, G. falsostuarti*], *G. gansseri, G. havanensis* (Fig. 7C), *C. plummerae* and others are not recorded in the upper part of the section.

The upper boundary of this zone was not identified in the studied section. It should continue higher into the marls of the overlying El Haria Formation. In section AM about 13 m of marls and limestones are attributed to the *G. gansseri* Zone.

The *G. gansseri* Zone was considered for a long time to be the middle zone of the Maastrichtian (Robaszynski et al., 1984; Caron, 1985; Sliter, 1989). However, after correlation of calcareous plankton biostratigraphy via magnetostratigraphy and ammonite stratigraphy, it was seen that it is latest Campanian–Early Maastrichtian in age (Premoli Silva and Sliter, 1995, 1999; Robaszynski and Caron, 1995; Hardenbol and Robaszynski, 1998; Robaszynski et al., 2000; Premoli Silva and Verga, 2004; Robaszynski and Mzoughi, 2010).

4.3. Calcareous nannofossils from the base of the Abiod Formation

Calcareous nannofossil assemblages are quite abundant but poorly preserved. The studied samples yielded a moderately diverse assemblage with an average of 25 species identified (see Table 1). The assemblages are dominated by low-latitude Tethyan taxa, although taxa of boreal affinity, such as *Orastrum campanensis*, occur sporadically.

For the present work we preferred to consider and discuss the most important biostratigraphic events and their succession rather than apply a "standard" zonation. This allows a more flexible comparison and long range correlation.

All the samples analyzed contain *Aspidolithus parcus parcus* and *Aspidolithus parcus constrictus* (Fig. 9B), which indicate an early Campanian age. Most nannofossil workers (Thierstein, 1976; Perch-Nielsen, 1985; Bralower et al., 1995; Gardin et al., 2001 and many others) agree in placing the base of the Campanian at the LO of *A. parcus parcus*, marker of CC18 Zone (Sissingh, 1977; Perch-Nielsen, 1985), NC 18 Zone (Roth, 1978) and UC 14 Zone (Burnett, 1998). A morphological lineage from *Aspidolithus parcus expansus* to *A. parcus parcus* and *A. parcus constrictus*, characterized by a reduction of the central-plate area, characterizes the uppermost Santonian–basal Campanian (Crux, 1982; Gardin et al., 2001). The "*A. parcus* Zone", marked by the occurrence of the nominate taxon, correlates well with the *Gt. elevata* Zone of planktonic foraminifera and Chron 33R at low latitudes (Bralower et al., 1995; Gardin et al., 2001).

Burnett (1998) erected a basal Campanian zone defined by the LO of *Aspidolithus cymbiformis* (UC13). This event, however, is not robust (see discussion in Wagreich et al., 2010). In our analysis *A. cymbiformis* (Fig. 9A) was found to be very rare, occurring only sporadically. A regular occurrence of *A. cymbiformis* l.s. was observed only above the LO of *A. parcus* in the Italian Bottaccione section (Gardin et al., 2001).

The occurrence of *Ceratholithoides verbeecki* (Fig. 9C) in sample AM10 indicates a slightly younger age; its LO was used by Perch-Nielsen (1985) to define subzone CC18b and by Burnett (1998) to define subzone UC14. The absence of *Ceratolithoides aculeus*, whose first occurrence is usually found within the former *G. ventricosa* Zone of planktonic foraminifera and Chron 33N at low latitudes (Bralower et al., 1995; Gardin et al., 2001), excludes a late-early Campanian age.

4.4. Chemostratigraphy: stable carbon isotopes

The $\delta^{13}C$ values of the Ain Medheker section range between 1.4‰ and 2.3‰ (Fig. 4). They are ca. 0.3‰ higher than those described by Jarvis et al. (2002) from El Kef (NW Tunisia) and from Trunch (England). Our biostratigraphic framework allows us to correlate three major excursions of $\delta^{13}C$ values that are documented in section AM (dotted areas of Fig. 4) with three major isotopic events sensu Jarvis et al. (2002): Santonian–Campanian Event (1), Mid-Campanian Event (5) and Upper Campanian Event (9). Moreover, two minor positive isotopic excursions (4, 8) and two minor negative isotopic excursions (2, 6) following the terminology of Jarvis et al. (2002) have been identified (Fig. 4) and allow for isotopic comparisons and further subdivision of the Abiod Formation. The correlation of isotopic events 3 and 7 with corresponding $\delta^{13}C$ values of section AM remains unclear. The following characteristics of the isotopic events of the section are summarized from bottom to top:

(1) A sharp increase in $\delta^{13}C$ values occurs at the base of the *G. elevata* Zone of section AM, corresponding with the Santonian–Campanian Event of the upper *Marsupites testudinarius* Zone in Trunch (Jarvis et al., 2002). This event defines a global positive $\delta^{13}C$ excursion and is reflected in a 6-m-thick interval of platy limestones with maximum $\delta^{13}C$ values of up to 2.3‰ in section AM (Fig. 4).

(2) A negative excursion above is indicated by a sharp decrease in $\delta^{13}C$ values in the middle part of the *G. elevata* Zone of section AM. It was correlated with the carbon isotopic event 2 of the upper part of the *Offaster pilula* Zone at Trunch (Fig. 4). This minor isotopic event is more pronounced at section AM, owing to a more rapid decrease to lower $\delta^{13}C$ values of 1.7‰ (Fig. 4). The increasing $\delta^{13}C$ values in section AM above, with maximum values of up to 2.3‰, have no counterparts at Trunch.

(3) The minor isotopic event 3 was defined by a small increase in $\delta^{13}C$ values near the base of *G. ventricosa* Zone in El Kef, corresponding to the lower *Gonioteuthis quadrata* Zone at Trunch (Jarvis et al., 2002). It may correlate with minor fluctuations of the $\delta^{13}C$ curve at section AM near sample 45 (upper part of the *G. elevata* Zone; Fig. 4). However, an unequivocal correlation of event 3 to section AM is hindered by clear assignments to the isotopic curve.

(4) Event 4 corresponds to a minimum of $\delta^{13}C$ values in the lower- to mid-*C. plummerae* Zone of both sections El Kef and AM, which was correlated to the middle *G. quadrata* Zone at Trunch (Jarvis et al., 2002).

(5) A prominent increase of $\delta^{13}C$ values followed by a long positive excursion corresponds to the Mid-Campanian Event (Jarvis et al., 2002). In El Kef the onset of that event lies near the top of the *C. plummerae* Zone, whereas it occurs in the middle part of that biozone in section AM, where it spans a 5-m-thick limestone interval. According to Jarvis et al. (2002, 2006), isotopic event 5 is correlated with the base of the Late Campanian *Belemnitella mucronata* Zone at Trunch (Fig. 4).

(6) A change to increasing $\delta^{13}C$ values (<2‰) in the upper part of the *C. plummerae* Zone at both sections AM and El Kef marks event 6, corresponding to the lower *B. mucronata* Zone of Trunch.

(7) A $\delta^{13}C$ trough in the lower *R. calcarata* Zone at El Kef section correlates to a break in slope in the lower *B. mucronata* Zone of Trunch (Jarvis et al., 2002). In section AM this tie point is not clearly visible, although a complete stratigraphic record (without turbidites and slumps) was assumed for the late *C. plummerae* to *R. calcarata* zones.

(8) A significant positive shift of $\delta^{13}C$ values in the lower *G. falsostuarti* Zone of both Tunisian sections is less pronounced at Trunch (Fig. 4). The LO of *R. hexacamerata* directly above this minor event confirms a good correlation between sections El Kef and AM.

(9) A major negative carbon isotope excursion marks the base of the *G. gansseri* Zone at El Kef and corresponds with the middle *B. mucronata* Zone at Trunch. Minimum $\delta^{13}C$ values (1.45‰) above the LO of *Gs. gansseri* are less pronounced in section AM (Fig. 4). The positive excursion above occurs in the topmost limestones of the Abiod Formation in Ain Medheker and correlates with the Upper Campanian Event sensu Jarvis et al. (2002).

All three major events 1, 5, and 9 show similar relative $\delta^{13}C$ fluctuations in all sections (Fig. 4). In section Am, the "Early Campanian Event" represents a positive carbon isotope excursion of around +0.3‰ and the Mid-Campanian Event an excursion of more than +0.2‰; the magnitudes of both events are closely comparable to those described by Jarvis et al. (2002). The negative carbon isotope excursion of −0.4‰ at the base of the "Late Campanian Event" (El Kef and Trunch) corresponds to −0.3‰ in section AM.

4.5. Facies characteristics

"Chalky" limestones are often described as representing the Abiod Formation (Burollet, 1956; Jarvis et al., 2002; Mabrouk et al., 2005). In the section AM, however, hard limestones prevail: "chalky" lithologies occur only in the upper part of the section, because of diagenetic alterations (compare Hennebert et al., 2009). The studied white–grey limestones and dark grey argillaceous limestones comprise pelagic/hemipelagic deposits, superimposed by submarine slides/slumps with intercalated sediment gravity flow deposits (turbidites). Similar facies types are described from various Abiod localities in Tunisia (Burollet, 1956; Negra, 1994; Negra and Zagrarni, 2007); however, some additional discussion for the Ain Medheker outcrop is required.

Four slumping intervals (comprising 2–11 slump beds) were separated by four turbidite-rich intervals (each comprising 1–4 turbidite beds) with gradational boundaries between both interval types (Fig. 2). These fourfold, alternating intervals indicate cyclic changes between two different mass-flow processes, submarine slides/slumps and gravity flows. Both, slumps and turbidites are missing from the topmost part of the section (near the Abiod–El Haria boundary).

Hemipelagic limestones. These represent the prevailing lithology of section AM. They are composed of cm- to dm-thick well-bedded limestones and marly limestones. Mudstones and wackestones dominate these hemipelagites, containing 10–20% planktonic foraminifera (Fig. 2, right-hand column), <2% benthonic foraminifera and generally <1% bioclasts plus quartz; the micritic matrix may reach more than 80% (Fig. 9G).

Slumps. Several slump beds of units III and IV are up to 3.5 m thick (Fig. 6). They are characterized by internal reworking, synsedimentary folding, and reworked clasts (Fig. 6A–C). Large m-scale cut

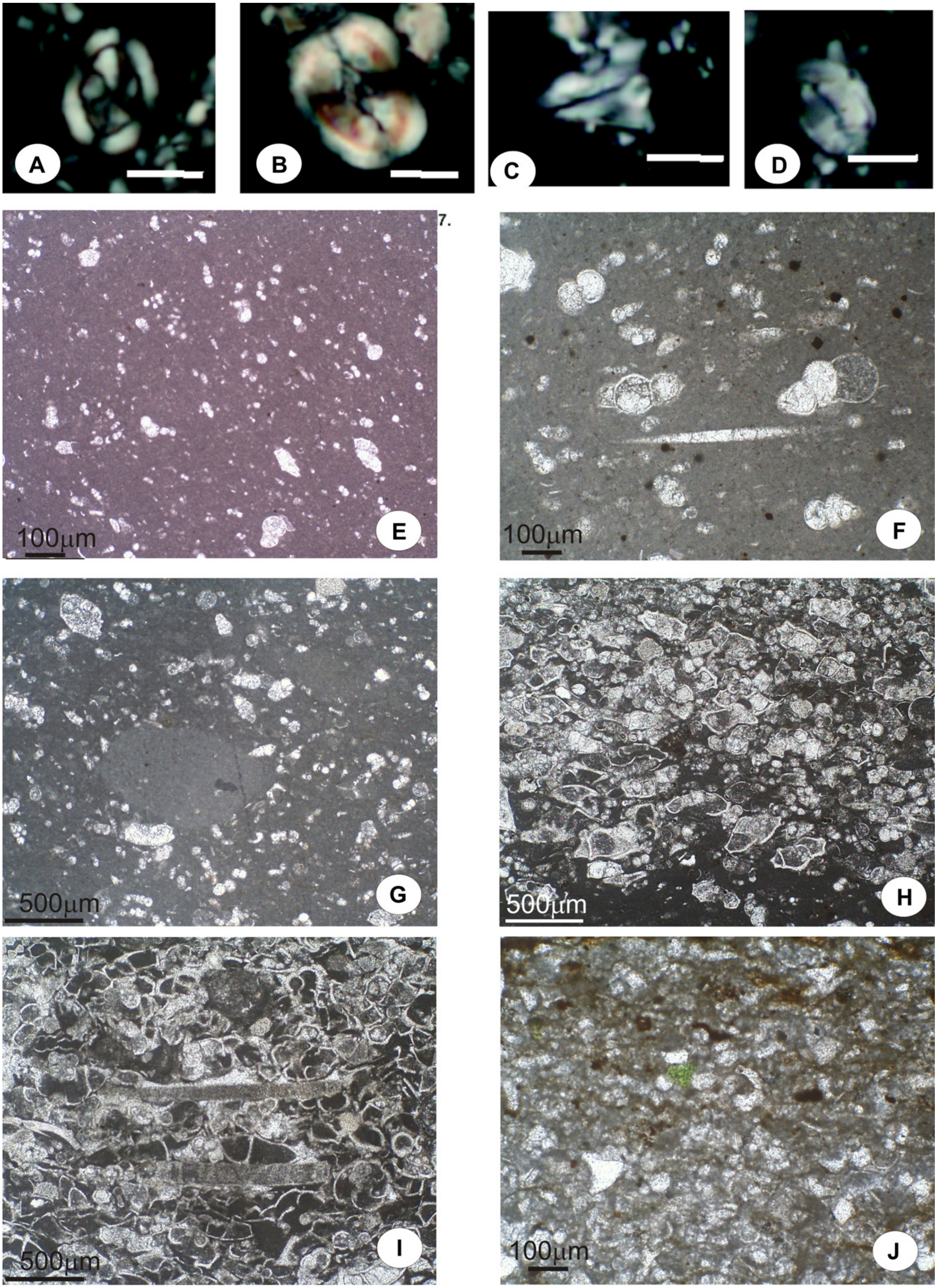
A
B
C
D
7.
100µm
E
100µm
F
500µm
G
500µm
H
500µm
I
100µm
J

and fill structures reflect mass transport processes of pre- to unconsolidated sediment bodies that were translocated downslope along discrete shear planes. Folding may be involved, often co-occurring with irregular dm-scale limestone nodules (Fig. 6C). As dewatering structures (resulting from squeezing out of excess water from pores during compaction) are missing, the folds argue for syndepositional slope instability. The varying strike and dip directions of some measured fold axes (with a centre of dip around northeast) indicate a southeast dipping palaeo-slope. The slumping structures did not disturb the general stratigraphic succession, thus indicating only minor vertical offsets during displacements at the slope. Similarly the slumps resulted only in a minor amalgamation that is stratigraphically not resolvable.

Turbidites. Sediment gravity flows are represented by turbidites, composed of cm-thick layers of packstones, irregularly cutting into unconsolidated wackestones below (Fig. 6E). Except for the lower turbidite (a), each of the three turbidite beds of section AM are summarized to one turbidite-rich interval; they alternate with four turbidite-free slumping intervals. The quantitative distribution of the main components determined in thin sections of single turbidite beds demonstrates a generally low content of quartz (0–3%) or glauconite (Fig. 9J), inoceramid remains (0–5%; Fig. 9I) (one turbidite sample (AM 51) with max. 8%), and benthonic foraminifera (0–2%: max. 3%), in contrast to the relative abundance of planktonic foraminifera (10–70%: max. 82%)[varying percentage values of the mainly micritic matrix were not considered for all volumetric calculations]. Most turbidites correlate with peaks of planktonic foraminiferal distribution, except f and h (Fig. 2). Increased quartz content occurs only in turbidites a, d, j, however, with low absolute values of 0.5–2.3%; many of the biogenic particles are fragmented (Melki and Negra, 2008), some are stained with iron oxides.

Similar grainstones of the Abiod Formation and its equivalent (Merfeg Formation) have often been interpreted as (calci)turbidites; however, we consider a possible alternative origin for those of Ain Medheker, taking into account microscopic results and palaeogeographic considerations. "Normal" turbidite sequences are usually composed of alternating proximal and distal turbidite beds (e.g., Ortner, 2001). The first are dm- to m-thick, often with internal grading and mostly composed of various particles that are often dominated by shelf-derived material with clastic admixtures, while the second are mm- to cm-thick (e.g., Flügel, 2004). The studied turbidites, however, show constant thicknesses of only up to 2 cm within the whole Abiod succession; bedding types are more irregular with diffuse base-contacts and bioturbation. Their petrographic and biogenic composition is nearly identical to the background sediment, but with higher concentrations of planktonic foraminifera.

We therefore conclude that the turbidites of Ain Medheker either represent bottom-current reworked turbidites, or contourites. Although differentiation between these is not easy (Stow et al., 1998; Sighinolfi and Tateo, 1998), they clearly differ from pure turbidites. Additional arguments for a non-pure turbidite interpretation come from the palaeogeographic position of the AM section close to a submarine swell (Fig. 1A): The turbidites of the section are not derived from shallow-water platform and platform-edge settings, but show a constant biogenic input from (hemi)pelagic environments, indicating solely deep water sources of allochthonous components (without land connection). Thus they may result from primary accumulations on submarine swells in upper slope environments and later transport along the slope. The observed constant minor bed thicknesses argue against a "normal" turbiditic origin with thickness- and grain-size changes along vertical sections, reflecting changes from proximal to distal positions.

The Abiod deposition of Ain Medheker took place in deeper shelf environments, periodically influenced by submarine slides/slumps and alternating with periods of increased debris flow deposits. Both mass-flow types were possibly caused by different mechanisms: major structural changes, earthquakes, or salt-derived forces are assumed to have activated the thick submarine slides and slumps, while the thin turbidites are interpreted to have been triggered by high rates of sedimentation in regions of dominant pelagic biogenic input. Bottom currents could have released accumulations of pelagic biota (possibly in areas of over-steep slopes), resulting in bottom-current, reworked turbidites, or in contourite deposits in a (south)easterly down-slope position of the submarine swell parallel to the "North–South Axis"-tectonic element.

4.6. Tectonic characteristics

The Late Cretaceous carbonates of the Abiod Formation of Ain Medheker were subdivided into seven mappable units I–VII (Fig. 2) that were deposited during two different tectonic regimes, A and B. Synsedimentary extensional movements prevailed during the Early Campanian (*G. elevata* Zone) of regime A (unit I), while no imprints of major tectonic activity occurred during the Middle Campanian–Early Maastrichtian tectonic regime B (equivalent to units II–VII of the *C. plummerae* to *G. gansseri* zones).

During tectonic regime A, a major normal fault (dipping 27° to the west) cross-cuts the well-bedded carbonates of unit I in the eastern part of the outcrop (Fig. 5A,B) with a vertical displacement of 15 m. Fault-activity stopped at the base of unit II, as indicated by horizontally bedded, undisturbed beds above (Fig. 5B). Within unit I, the three bedded couplets a, b, and c show a gradual thickening towards the fault and at the same time a characteristic drain off to the west (Fig. 5A,B). No rotation of the down-dropped block is visible and thus records syndepositional fault motion and filling of the small graben during the Early Campanian extensional event. Thickness changes across a synsedimentary fault (i.e., growth fault) record differences in elevation of the depositional surface on the footwall and hanging-wall sides of the fault through time. These thickness changes, although modified by compaction, allow the determination of fault throws subsequent to the deposition of each horizon, and hence the reconstruction of the history of fault movement.

Consequently, we assume a local submarine asymmetric graben to be filled with basal Abiod sediments during tectonic regime A, reflecting a N–NE striking graben axis that runs perpendicular/oblique to extensional stress-fields arranged more or less in a NNW–SSE direction.

A comparable tectonic evolution was described by Mabrouk et al. (2005) for the offshore Miskar structure of the Pelagian Shelf. Based on seismic interpretations, these authors identified a major extensional structure formed during the same time interval within an extensional tectonic stress-field. Dlala (2002) similarly demonstrated for southern Tunisia that extensive tectonic processes persisted until the Campanian–Maastrichtian, evidenced by several synsedimentary normal faults, associated with basaltic lavas. He suggested that the east–west transform fault of the North

Fig. 9. Nannofossils and microfacies of the Abiod Formation of Ain Medheker. A, *Aspidolithus cymbiformis* (sample AM 23), scale 5 μm. B, *Aspidolithus parcus constrictus* (AM 7), scale 5 μm. C, *Ceratolithoides verbeecki* (AM 10), scale 5 μm. D, *Orastrum campanensis* (AM 13), scale 5 μm. E, Wackestone of a slumped unit (AM 65). F, Sponge spicule in wackestones of a slumped unit (AM 73). G, mud extraclast in non-turbiditic wackestones (AM 79). H, turbiditic foraminiferal packstone with erosive base (AM 49). I, foraminiferal packstone with inoceramid remains of a turbiditic layer (AM 120). J, glauconite and quartz grains of turbiditic wacke/packstones (AM 26a).

African margin remained active during this period. Syntectonic deposition resulting from combined strike-slip and normal faults, and associated thickness variations have also been described form elsewhere in North Africa during this interval (Guiraud and Bosworth, 1997, 1999).

5. Conclusions

Planktonic foraminifera identified in thin sections and calcareous nannofossils of the Late Cretaceous Abiod Formation of Ain Medheker enable the identification of the following biozones: *G. elevata, C. plummerae* (replacing the former *G. ventricosa* Zone), *R. calcarata, G. falsostuarti*, and *G. gansseri*, spanning in age from Early Campanian to Early Maastrichtian.

The combination of biostratigraphic and chemostratigraphic data allowed the identification of three major isotopic events: the Santonian–Campanian Boundary Event, the Mid-Campanian Event, and the Late Campanian Event. They underline (together with four minor isotopic events) the stratigraphic similarities between the western (El Khef) and eastern (Ain Medheker) Tunisian realms.

Deposition of the studied section AM was influenced by several mass-flow processes; periods with submarine slides/slumps (gliding towards the southeast) alternate with turbidite intervals, probably caused by bottom-current reworking (contourites). The primary causes for these mass-flow systems may have resulted either from semi-consolidated carbonate material on the slopes or from seismic events, owing to tectonic activity.

The Early Campanian deposition of Ain Medheker was controlled by synsedimentary extensional tectonics (submarine fault-controlled half-graben) that ceased later during Late Campanian times. The observed asymmetrical half-graben may represent a segment of a larger negative flower structure that was inverted during the Miocene compressional regime. Thus, it represents an "original" extensional structure of Late Cretaceous age that is preserved in the "North–South Axis"-tectonic element.

Acknowledgements

BS thanks DAAD (German Academic Exchange Office), Bonn for a 2-year grant to stay at Bremen University. DAAD also supported the fieldwork of JK. We thank Dr. Monika Segl, MARUM Bremen for isotope measurements and Ralf Bätzel, Bremen, for preparation of thin-sections. Many thanks are also extended to S. Melki, Tunis for introducing us to the section. Two anonymous referees are thanked for their constructive reviews.

References

Abdallah, H., 1987. Le Crétacé supérieur de la Chaîne Nord des chotts (Sud Tunisien). Biostratigraphy, sédimentation, diagenèse. Doctoral Thesis, University of Dijon, 255 pp.

Anderson, J.E., 1996. The Neogene structural evolution of the western margin of the Pelagian Platform, central Tunisia. Journal of Structural Geology 18, 819–833.

Baird, D.W., Aburawi, R.M., Bailey, J.L., 1996. Geohistory and petroleum in the central Sirt Basin. In: Salem, M.J., Busrewil, M.T., Misallati, A.A., Sola, M.A. (Eds.), The Geology of Sirt Basin, vol. 3, pp. 3–56.

Ben Ferjani, A., Burollet, P.F., Mejri, F., 1990. Petroleum Geology of Tunisia. Entreprise Tunisienne des Activités Pétrolières, Tunis, 194 p.

Boccaletti, M., Cello, G., Tortorici, L., 1988. Structure and tectonic significance of the North–South axis. Annales Tectonicae 2, 12–20.

Bouaziz, S., Barrier, E., Soussi, M., Turki, M.M., Zouari, H., 2002. Tectonic evolution of the northern African margin in Tunisia from paleostress data and sedimentary record. Tectonophysics 357, 227–253.

Bralower, T.J., Leckie, R.M., Sliter, W.V., Thierstein, H.R., 1995. An integrated Cretaceous microfossil biostratigraphy. In: Berggren, W. (Ed.), Geochronology, Time Scales and Global Stratigraphic Correlation. Society of Economic Paleontologists and Mineralogists, Special Publication, vol. 54, pp. 65–79.

Burnett, J.A., with contributions from Gallagher, L.T., Hampton, M.J., 1998. Upper Cretaceous. In: Bown, P.R. (Ed.), Calcareous Nannofossil Biostratigraphy. British Micropalaeontological Society Publications Series, Chapman and Hall, London, pp. 132–198.

Burollet, P.F., 1956. Contribution à l'étude stratigraphique de la Tunisie Centrale. Annales des Mines et de la Géologie 18, 388. Tunis.

Burollet, P.F., Ellouz, N., 1984. L'évolution des bassins sédimentaires de la Tunisie centrale et orientale. Bulletin Centre Recherche Exploration-Production Elf Aquitaine 10, 49–68.

Caron, M., 1978. Cretaceous Plankton Foraminifers from DSDP Leg 40, Southeastern Atlantic Ocean. In: Initial Reports of the Deep Sea Drilling Project, vol. 40 651–678.

Caron, M., 1985. Cretaceous planktic foraminifera. In: Bolli, H.M., Saunders, J.B., Perch-Nielsen, K. (Eds.), Plankton Stratigraphy. Cambridge University Press, Cambridge, pp. 17–86.

Chaabani, F., 1994. Variations sédimentaire sous contrôle tectonique durant le Sénonian supérieur au niveau de la passe de Chemsi (Tunisie méridionale): cadre océanographique et implications paléogéographiques. In: Proceedings, 4th Tunisian Petroleum Exploration Conference, vol. 7. Entreprise Tunisienne d'Activités Pétrolières, Tunis, pp. 443–457.

Crux, J.A., 1982. Upper Cretaceous (Cenomanian to Campanian) calcareous nannofossils. In: Lord, A.R. (Ed.), A Stratigraphical Index of Calcareous Nannofossils. British Micropalaeontological Society Series, pp. 81–135. London.

Dlala, M., 2002. Les manifestations tectono-sédimentaires d'âge Campanien–Maastrichtien en Tunisie: implications sur l'évolution géodynamique de la marge Nord-Africaine. Comptes Rendus Geoscience 334, 135–140.

Flügel, E., 2004. Microfacies of Carbonate Rocks: Analysis, Interpretation and Application. Springer, Berlin-Heidelberg, 983 pp.

Gardin, S., Del Panta, F., Monechi, S., Pozzi, M., 2001. A tethyan reference section for the Campanian and Maastrichtian stages: the Bottaccione section (Central Italy). Review of the data and new calcareous nannofossil results. In: Odin, G.S. (Ed.), The Boundary between the Campanian and the Maastrichtian Stages: Characterisation and Correlation from Tercis-lesbains to Europe and Other Continents. Developments in Paleontology and Stratigraphy, vol. 19, pp. 820–833.

Gradstein, F., Ogg, J., Smith, A., 2004. A Geologic Time Scale. Cambridge University Press, Cambridge, 589 pp.

Guiraud, R., 1998. Mesozoic rifting and basin inversion along the northern African Tethyan margin: an overwiew. In: MacGregor, D.S., Moody, R.T.J., Clark-Lowes, D.D. (Eds.), Petroleum Geology of North Africa. Geological Society, London, Special Publication, vol. 133, pp. 217–229.

Guiraud, R., Bosworth, W., 1997. Senonian basin inversion and rejuvenation of rifting in Africa and Arabia: synthesis and implications to plate-scale tectonics. Tectonophysics 282, 39–82.

Guiraud, R., Bosworth, W., 1999. Phanerozoic geodynamic evolution of northeastern Africa and the northwestern Arabian platform. Tectonophysics 315, 73–108.

Hardenbol, J., Robaszynski, F., 1998. Introduction to Upper Cretaceous. In: de Graciansky, P.C., et al. (Eds.), Mesozoic and Cenozoic Sequence Stratigraphy of European Basins. SEPM (Society for Sedimentary Geology), Special Publication, vol. 60, pp. 329–332.

Hennebert, M., Robaszynski, F., Goolaerts, S., 2009. Cyclostratigraphy and chronometric scale in the Campanian–Lower Maastrichtian: the Abiod Formation at Elle's, central Tunisia. Cretaceous Research 30, 325–338.

Jacobs, L.L., Ferguson, K., Polcyn, M.J., Rennison, C., 2005. Cretaceous $\delta^{13}C$ stratigraphy and the age of dolichosaurs and early mosasaurs. Geologie en Mijnbouw 84, 257–268.

Jarvis, I., Gale, A., Jenkyns, H.C., Pearce, M.A., 2006. Secular variations in Late Cretaceous carbon isotopes: a new $\delta^{13}C$ carbonate reference curve for the Cenomanian–Campanian (99.6–70.6 Ma). Geological Magazine 143, 561–608.

Jarvis, I., Mabrouk, A., Moody, R.T.J., de Cabrera, S., 2002. Late Cretaceous (Campanian) carbon isotope events, sea-level change and correlation of the Tethyan and Boreal realms. Palaeogeography, Palaeoclimatology, Palaeoecology 188, 215–248.

Khessibi M., 1978. Etudes géologiques du secteur de Maknassi-Mezzouna et du Djebel Kébar (Tunisie centrale). Thesis, University of Lyon, 175 pp.

Khomsi, S., Ben Jemia, M.G., Frizon de Lamotte, D., Maherssi, C., Echihi, O., Mezni, R., 2009. An overview of the Late Cretaceous–Eocene positive inversions and Oligo-Miocene subsidence events in the foreland of the Tunisian Atlas: structural style and implications for the tectonic agenda of the Maghrebian Atlas system. Tectonophysics 475, 38–58.

Klett, T.R., 2001. Total petroleum systems of the Pelagian Province, Tunisia, Libya, Italy and Malta –The Bou Dabbous– Tertiary and Jurassic–Cretaceous composite. United States Geological Survey, Bulletin 2202-D, 27 pp. + appendices.

Li, L., Keller, G., 1998. Diversification and extinction in Campanian-Maastrichtian planktic foraminifera of northwestern Tunisia. Eclogae Geologicae Helvetiae 91, 75–102.

Li, L., Keller, G., Adatte, T., Stinnesbeck, W., 2000. Late Cretaceous sea-level changes in Tunisia: a multi-disciplinary approach. Journal Geological Society London 157, 447–458.

Li, L., Keller, G., Stinnesbeck, W., 1999. The Late Campanian and Maastrichtian in northwestern Tunisia: palaeoenvironmental inferences from lithology, macrofauna and benthic foraminifera. Cretaceous Research 20, 231–252.

Mabrouk, A., Belayouni, H., Jarvis, I., Moody, R.T.J., 2006. Strontium, $\delta^{18}O$ and $\delta^{13}C$ as palaeo-indicators of unconformities: case of the Aleg and Abiod formations (Upper Cretaceous) in the Miskar Field, southeastern Tunisia. Geochemical Journal 40, 405–424.

Mabrouk, A., Jarvis, I., Belayouni, H., Moody, R.T.J., de Cabrera, S., 2005. An integrated chemostratigraphic study of the Campanian–Early Maastrichtian deposits of the Offshore Miskar Field in southeastern Tunisia: SIS, $\delta^{13}C$ and $\delta^{18}O$ isotopes, and elemental geochemistry. Stratigraphy 2, 193–216.

Melki, S., Negra, M.H, 2008. The Abiod Formation in the Enfida area: particular sedimentary features and reservoir properties and implications. Tunis Petroleum Exploration Conference. Tunis ETAP Memoir 27, 129–137.

M'Rabet, A., Negra, M.H., Purser, B.H., Sassi, S., Ben-Ayed, N., 1986. Micrite diagenesis in Senonian rudist buildups in central Tunisia. In: Purser, B.H., Schröder, J.H. (Eds.), Reef Diagenesis. Springer-Verlag, Berlin, pp. 210–223.

Negra, M.H., 1986. Paleoenvironment et conditions de genese du compleve senonien recifal a rudistes du Jebel el Kebar, Tunisie central. Bulletin de la Société Geologique de France (8) 3 (2), 317–326.

Negra, M.H., 1994. Les dépôts de plate-forme à bassin du Crétacé supérieur en Tunisie Centro-septentrionale (Formation Abiod et facies associés). Stratigraphie, sédimentation, diagenèse et intérêt pétrolier. DSc Thesis, University of Tunis, 649 pp.

Negra, M.H., 1995. La trilogie de la formation Abiod: origines et signification sédimentologique de son absence. 3e Congrès naturale des Sciences de la Terre, Tunis. Société des Sciences de la Terre, Tunisie, p. 125.

Negra, M.H., Gili, E., 2004. The role of rudists in micrite production and stabilisation. Example of the Upper Cretaceous rudist formations in Jebel el Kebar, Central Tunisia. Courier Forschungsinstitut Senckenberg 247, 193–205.

Negra, M.H., M'Rabet, A., 1994. The Abiod facies, reparition and reservoir aspects. In: Proceedings, 4th Tunisian Petroleum Exploration Conference, Tunis, vol. 7. Entreprise Tunisienne d'Activités Pétrolières, Mémoire, pp. 495–507.

Negra, M.H., Purser, B.H., 1989. Les monticules senoniens a rudistes du Jebel el Kebar, Tunisie Centrale. Anatomie, diagenese et geometrai. Géologie Méditerranéene 16, 99–119.

Negra, M.H., Purser, B.H., 1995. Upper Cretaceous carbonate platform margins in Central-North Tunisia. IAS, 17th Regional Meeting of Sedimentology, Sfax, Tunisia, Excursion B4, Field Trip Guide Book, 27 pp.

Negra, M.H., Purser, B.H., M'Rabet, A., 1995. Sedimentation, diagenesis and syntectonic erosion of Upper Cretaceous rudist mounds in Central Tunisia. In: Monty, C.L.V., Bosence, D.W.J., Bridges, P.H., Pratt, B.R. (Eds.), Special Publication of the International Association of Sedimentologists, vol. 23, pp. 401–419.

Negra, M.H., Zagrarni, M.F., 2007. Upper Cretaceous tempestites in rudist-rich facies, Tunisia. In: Scott, R. (Ed.), Cretaceous Rudists and Carbonate Platforms: Environmental Feedback. SEPM (Society for Sedimentary Geology), Special Publication, vol. 87, pp. 45–56.

Ortner, H., 2001. Growing folds and sedimentation of the Gosau Group, Muttekopf, northern Calcareous Alps, Austria. International Journal of Earth Sciences 90, 727–739.

Ouali, J., Tricart, P., Delteil, J., 1987. Ampleur et signification des recouvrements anormaux dans l'axe Nord–Sud (Tunisie centrale: donnees nouvelles dans le chainon Nara-Sidi Khalif). Eclogae Geologicae Helveticae 80, 685–696.

Perch-Nielsen, K., 1985. Mesozoic calcareous nannofossils. In: Bolli, H.M., Saunders, J.B., Perch-Nielsen, K. (Eds.), Plankton Stratigraphy. Cambridge University Press, Cambridge, pp. 329–426.

Petrizzo, M.R., 2000. Upper Turonian–lower Campanian planktonic foraminifera from southern mid-high latitudes (Exmouth Plateau, NW Australia): biostratigraphy and taxonomic notes. Cretaceous Research 21, 479–505.

Petrizzo, M.R., 2001. Late Cretaceous planktonic foraminifera from Kerguelen Plateau (ODP Leg183): new data to improve the Southern Ocean biozonation. Cretaceous Research 22, 829–855.

Petrizzo, M.R., 2003. Late Cretaceous planktonic foraminiferal bioevents in the Tethys and in the Southern Ocean record: an overview. Journal of Foraminiferal Research 33, 330–337.

Petrizzo, M.R., Falzoni, F., Premoli Silva, I., 2011. Identification of the base of the lower-to-middle Campanian *Globotruncana ventricosa* Zone: comments on reliability and global correlations. Cretaceous Research 32, 387–405.

Postuma, J.A., 1971. Manual of Planktonic Foraminifera. Elsevier, Amsterdam, 420 pp.

Premoli Silva, I., Sliter, W.V., 1995. Cretaceous planktonic foraminiferal biostratigraphy and evolutionary trends from the Bottaccione Section, Gubbio, Italy. Palaeontographia Italica 82, 1–89.

Premoli Silva, I., Sliter, W.V., 1999. Cretaceous paleoceanography: evidence from planktonic foraminiferal evolution. In: Barrera, E., Johnson, C.C. (Eds.), Evolution of the Cretaceous Ocean-climate System. Geological Society of America. Special Paper, vol. 332, pp. 301–328.

Premoli Silva, I., Verga, D., 2004. Practical manual of Cretaceous planktonic foraminifera. In: Verga, D., Rettori, R. (Eds.), International School on Planktonic Foraminifera, 3rd Course: Cretaceous. Universities of Perugia and Milan, Tipografia Pontefelcino, Perugia.

Robaszynski, F., Caron, M., 1995. Foraminifères planctoniques du Crétacé: commentaire de la zonation Europe-Méditerranée. Bulletin de la Société Géologique de France 166, 681–692.

Robaszynski, F., Caron, M., Gonzalez, J.M., Wonders, A., 1984. Atlas of Late Cretaceous planktonic foraminifera. Revue de Micropaléontologie 26, 145–305.

Robaszynski, F., Gonzales Donoso, J.M., Linares, D., Amedro, F., Caron, M., Dupuis, C., Dhondt, A.V., Gartner, S., 2000. Le Crétacé supérieur de la région de Kalaat Senan, Tunisie centrale. Litho-biostratigraphie intégrée: zones d'ammonites, de foraminifères planctoniques et de nannofossiles du Turonien supérieur au Maastrichtien. Bulletin des Centres de Recherche Exploration-Production Elf-Aquitaine 22, 359–490.

Robaszynski, F., Mzoughi, M., 2004. La limite Campanien–Maastrichtien à Elles: une ligne temps pour corréler la Tunisie et de stratotype international de Tercis (France). In: Intérêt pétrolier. 19th Tunisian Petroleum Exploration and Production Conference. Entreprise Tunisienne d'Activité Pétrolière, Tunis, October 4–8, 2004, pp. 34–35.

Robaszynski, F., Mzoughi, M., 2010. L'Abiod d'Elles (Tunisie): stratigraphie, limite Campanien–Maastrichtien et correlation. Carnets de Geologie/Notebooks on Geology, 55. Article 2010/04 (CG2010_A04).

Roth, P.R., 1978. Cretaceous Nannoplankton Biostratigraphy and Oceanography of the Western Atlantic Ocean. In: Initial Reports of the Deep Sea Drilling Project, Leg, vol. 44 731–760.

Scholle, P.A., Arthur, M.A., 1980. Carbon isotope fluctuations in Cretaceous pelagic limestones: potential stratigraphic and petroleum exploration tool. American Association of Petroleum Geologists, Bulletin 64, 67–87.

Sighinolfi, G.P., Tateo, F., 1998. Mineralogical and geochemical criteria for distinguishing turbidite and hemipelagic pelites – the Maastrichtian of the northern Apennines, Italy. Sedimentary Geology 115, 301–313.

Sissingh, W., 1977. Biostratigraphy of Cretaceous calcareous nannoplankton. Geologie en Minjbouw 56, 37–65.

Sliter, W.V., 1989. Biostratigraphic zonation for Cretaceous planktonic foraminifers examined in thin section. Journal of Foraminiferal Research 19, 1–19.

Stow, D.A.V., Faugères, J.-C., Viana, A., Gonthier, E., 1998. Fossil contourites: a critical review. Sedimentary Geology 115, 3–31.

Thierstein, H.R., 1976. Mesozoic calcareous nannoplankton biostratigraphy of marine sediments. Marine Micropaleontology 14, 325–362.

Wagreich, M., Summesberger, H., Kroh, A., 2010. Late Santonian bioevents in the Schattau section, Gosau Group of Austria – implications for the Santonian–Campanian boundary stratigraphy. Cretaceous Research 31, 181–191.